Solar Physics (2006) 237: 85–100
DOI: 10.1007/s11207-006-0173-7

IS PRE-ERUPTIVE NULL POINT RECONNECTION REQUIRED FOR TRIGGERING ERUPTIONS?

HUI LI
Purple Mountain Observatory, 2 West Beijing Road, Nanjing 210008, China
(e-mail: lihui@mail.pmo.ac.cn)

BRIGITTE SCHMIEDER and GUILLAUME AULANIER
Observatoire de Paris, Section de Meudon, LESIA, F-92195, Meudon Principal Cedex, France

and

ARKADIUSZ BERLICKI
Astronomical Institute, Wrocław University, ul.Kopernika 11, 51-622 Wrocław, Poland

(Received 10 March 2006; accepted 10 June 2006; Published online 8 August 2006)

Abstract. We study the magnetic field evolution and topology of the active region NOAA 10486 before the 3B/X1.2 flare of October 26, 2003, using observational data from the French–Italian THEMIS telescope, the Michelson Doppler Imager (MDI) onboard Solar and Heliospheric Observatory (SOHO), the Solar Magnetic Field Telescope (SMFT) at Huairou Solar Observation Station (HSOS), and the Transition Region and Coronal Explorer (TRACE). Three dimensional (3D) extrapolation of photospheric magnetic field, assuming a potential field configuration, reveals the existence of two magnetic null points in the corona above the active region. We look at their role in the triggering of the main flare, by using the bright patches observed in TRACE 1600 Å images as tracers at the solar surface of energy release associated with magnetic reconnection at the null points. All the bright patches observed before the flare correspond to the low-altitude null point. They have no direct relationship with the X1.2 flare because the related separatrix is located far from the eruptive site. No bright patch corresponds to the high-altitude null point before the flare. We conclude that eruptions can be triggered without pre-eruptive coronal null point reconnection, and the presence of null points is not a sufficient condition for the occurrence of flares. We propose that this eruptive flare results from the loss of equilibrium due to persistent flux emergence, continuous photospheric motion and strong shear along the magnetic neutral line. The opening of the coronal field lines above the active region should be a byproduct of the large 3B/X1.2 flare rather than its trigger.

1. Introduction

Energy to power a solar eruption is generally thought to be stored in non-potential stressed and/or sheared magnetic fields. Hagyard (1990) pointed out that the existence of magnetic shear is a sufficient condition for getting a solar flare: the maximum shear angle along the neutral line is larger than 85° and the length of neutral line with shear angle $\geq 80°$ exceeds 8000–10 000 km. The required high shear can result from shearing motions in the photosphere, flux emergence or cancelling. Magnetic shear before and shear change during solar flares have been extensively studied (e.g., Sakurai *et al.*, 1992; Ambastha, Hagyard, and West, 1993; Wang *et al.*, 1994; Li *et al.*, 2000).

The high degree of magnetic complexity of an active region is a favorable condition required for the strong solar activity, as reviewed by Schmieder and van Driel (2005). Antiochos (1998) presented a reasonable explanation for the well-known observational complexity of solar magnetic field required to produce strong solar activity such as large eruptive solar flares. The analysis of magnetic topology of active regions tells us possible locations for magnetic reconnection where the stored energy can be released. These locations are the intersections of magnetic surfaces: the separatrices (with null points) or quasi-separatrices if the gradients of field line connectivity are not discontinuous, although these gradients are very strong (Démoulin *et al.*, 1997). Theoretical magnetohydrodynamical flare models are based on the existence of null points. For example, Antiochos, DeVore, and Klimchuk (1999) and DeVore and Antiochos (2005) proposed the so-called 'breakout' model. In this model, the magnetic field lines overlying the stressed magnetic regions break before the main flare and reconnect at a null point, involving multiple flux systems and shear concentrated near the neutral line. The stored energy is evacuated during a second phase named the impulsive phase.

Magnetic field configuration near a null point typically shows a fan and a spine structures. Fan and spine reconnection solutions around a magnetic null have been obtained both numerically (Craig and Fabling, 1996; Craig *et al.*, 1999) and analytically (Ji and Song, 2001). Some eruptive events show evidence for the existence of magnetic null points due to the complexity of field lines in the active region (e.g., Aulanier *et al.*, 2000; Démoulin and Klein, 2000; Manoharan and Kundu, 2005). Filippov (1999) observed a typical fan-spine structure near the solar limb with SOHO/EIT and showed that null points can be present in the corona, which appear dark in 195 Å and *Yohkoh* soft X-ray images with surrounding bright loops, suggestive of lower temperature and/or lower plasma density in the vicinity of the null point. More observations are needed to observationally confirm the existence of a magnetic null point, to illustrate its relation to magnetic reconnection, and to demonstrate the relation between magnetic reconnection near the null point and solar flares.

On October 26, 2003, a large 3B/X1.2 flare occurred in the active region (AR) NOAA 10486. Complicated radio spectra (Ning *et al.*, 2006) and a fast CME (Qiu *et al.*, 2006) were associated with this flare. Multiple wavelength analysis of this flare has been done by Li *et al.* (2005). In this paper, we study the magnetic configuration and topology of AR 10486 before the 3B/X1.2 flare. We will introduce the observations and data in Section 2 and describe the magnetic field structures in Section 3. Study of the magnetic topology and TRACE EUV observations are given in Sections 4 and 5, while in the last section (Section 6) we will present our discussion and conclusions.

2. Observations and Data

The *Solar Geophysical Data* (SGD) indicates that the 3B/X1.2 flare started at 05:57 UT, peaked at 06:54 UT, and ended at 07:33 UT of October 26, 2003, in

X-rays. This flare was observed by a few ground-based and space-borne instruments (see Li *et al.* (2005) for details). In this paper, we use the data from the French-Italian THEMIS telescope, the Huairou Video Vector Magnetograph (HVVM) mounted on the Solar Magnetic Field Telescope (SMFT) at Huairou Solar Observation Station (HSOS) of National Astronomical Observatories of China (NAOC) (Ai and Hu, 1986), the Michelson Doppler Imager (MDI) (Scherrer *et al.*, 1995) onboard the Solar and Heliospheric Observatory (SOHO) (Domingo, Fleck, and Poland, 1995), and the Transition Region and Coronal Explorer (TRACE) (Handy *et al.*, 1999).

Magnetic field data used in this paper were obtained by THEMIS, HVVM, and SOHO/MDI. The spectro-polarimetric observations of the flare were made by the THEMIS telescope with the MSDP spectrograph in the period of 07:46–8:56 UT, partially covering the gradual phase of the flare. THEMIS is a polarization-free telescope, designed especially for polarimetric observations. With the MSDP we can observe the Stokes parameter $I \pm V$ in the Na I 5896 Å line and deduce the longitudinal magnetic field (Mein, 2002).

The HVVM has been updated in recent years, and now it has a field-of-view (FOV) of about $225'' \times 170''$ with a pixel size of $0.35''$. The actual pixel size in this study was set to be $0.5''$ by binning the data in the calibration process so as to compare and align calibrated magnetograms with images from TRACE observation. The vector magnetic fields were derived from the measurements of the four Stokes parameters I, Q, U, and V. The transverse fields (parameters Q and U) were observed at the Fe I 5324.19 Å line center, and the longitudinal ones (parameter V) at 0.075Å from the Fe I 5324.19 Å line center.

MDI obtained the longitudinal magnetic field of the full solar disk in the Ni I 6768 Å line. The calibrated longitudinal field data with 1 min cadence are used in this paper to compute the magnetic flux of the active region and to make 3D extrapolation coupled with THEMIS observations.

UV and EUV data come from TRACE, which observed AR 10486 all the day on October 26, 2003, mainly in 195 Å (Fe XII) and 1600 Å with a format of 768×768 pixels, and occasionally in 284 Å with a format of 512×512 pixels, allowing us to carefully study the whole flare process, including the pre-flare evolution. The TRACE 195 and 1600 Å images were recorded with a cadence of about 50 s and a spatial resolution of $0.5''$, except for the period around the flare maximum from ≈06:10 to ≈06:40 UT, during which the 195 Å images were recorded with a higher temporal resolution (cadence of 15 s on average). The images were corrected for cosmic rays and differential rotation of the Sun using the TRACE software package in SolarSoft (*http://www.lmsal.com/solarsoft/*) so that they are well co-aligned with each other.

3. Magnetic Field Structure

AR 10486 (S17, L283) is one of the three main flare-productive regions that appeared in the period of October 18, 2003, through November 4 (Zhang *et al.*, 2003),

and produced 7 X-class flares (including the largest X28 flare in GOES observational history) and 15 M-class flares during this period. This AR is characterized of strong magnetic shear, successive flux emergence, continuous sunspot rotation, and complicated magnetic topology.

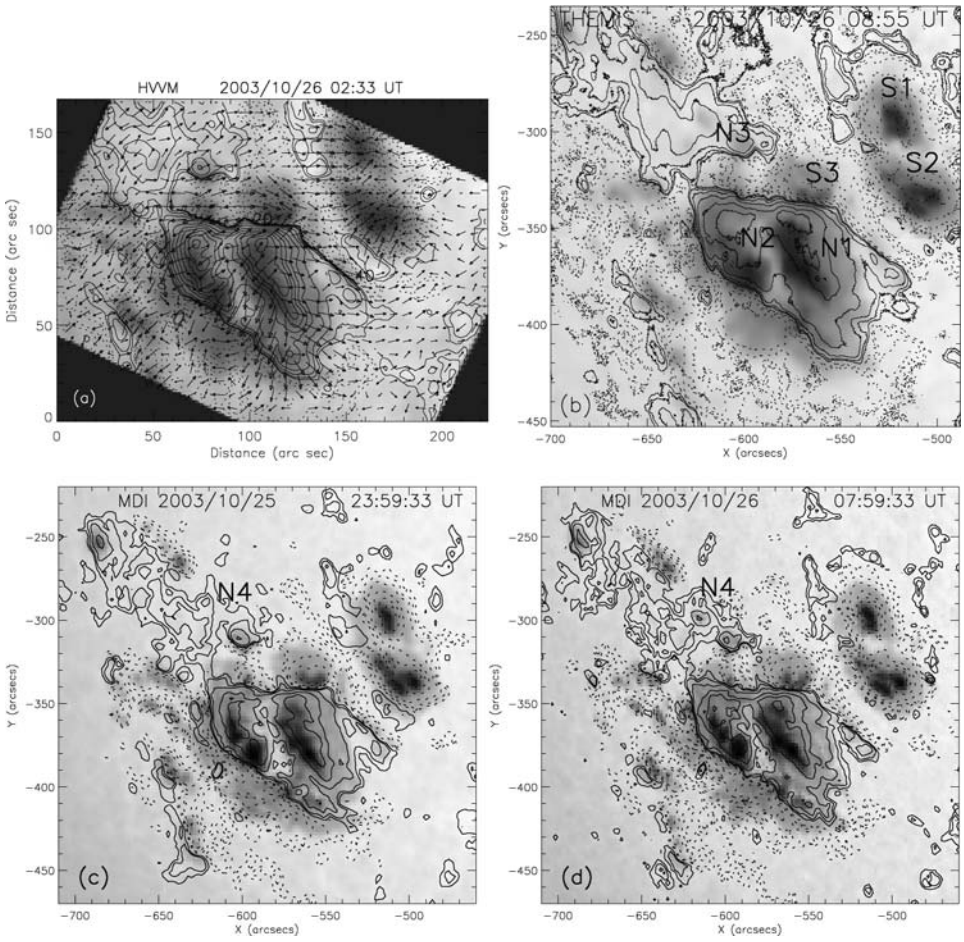

Figure 1. (a) Vector magnetogram obtained by HVVM at 02:33 UT on October 26, 2003. The *arrows* show the transverse field. The dark thick line in the middle part indicates the neutral line discussed in this paper. (b) Longitudinal magnetic field (*contours*) observed by THEMIS in MSDP mode starting at 08:55 UT. (c) and (d) Longitudinal magnetic field (*contours*) observed by SOHO/MDI at 23:59:33 UT of October 25 and 07:59:33 UT on October 26, respectively. The *solid/dotted contours* show the positive/negative longitudinal field with levels ±40, 80, 160, 320, 640, 960, 1280, 1600, 1920 Gauss. The background is the corresponding intensity image. Letters 'S1'–'S3' and 'N1'–'N3' in frame (b) mark regions of negative and positive polarities, respectively. North is on the top and east to the left. We will keep this convention for all the images shown in this paper.

Figure 1 shows the vector magnetogram of AR 10486 obtained at 02:33 UT by HVVM (frame (a)), and the longitudinal magnetic field observed by THEMIS in MSDP mode in the Na I 5896 Å line in 25 min scanning starting at 08:55 UT (frame (b)). The corresponding photospheric images of this active region are shown as the background images in the figure. The active region consisted of two main leading sunspots, S1 and S2, of negative polarity and two main following sunspots, N1 and N2, of positive polarity. Many satellite sunspots with different polarities appeared in the region, some of which shared the penumbrae with the main sunspots, forming the δ configuration of the active region (Figure 1). Two MDI longitudinal magnetograms obtained at 23:59:33 UT of October 25 and 07:59:33 UT of October 26 are also shown in Figure 1 (frames (c) and (d), respectively). By comparing the two magnetograms we see that flux emergence occurred mainly in the north-east part of this AR, as revealed, for example, by the region marked 'N4' in frames (c) and (d), which display an apparent increase of positive fields. Meanwhile, some magnetic islands in frame (c) showed decreased field strength in frame (d) or even disappeared, indicative of possible magnetic cancellation.

MDI intensity movie shows that motion and counter-clockwise rotation of the sunspots and flux emergence were in succession in this region. We quantitatively computed the sunspot rotation. Before computing, we corrected the MDI intensity images for both the differential rotation of the Sun and the projection effect. Let ψ to be the angle between the X-axis and the line connecting the intensity-weighted centers of S1 and S2 (Figure 2(a)), and measure it counter-clockwise from the

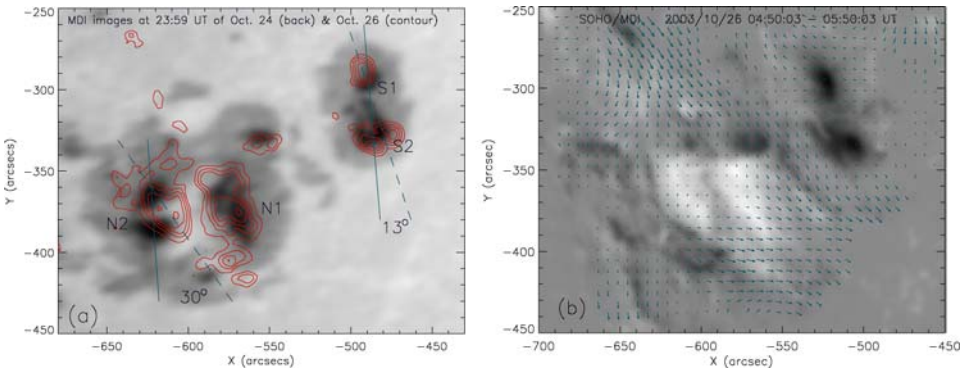

Figure 2. (a) MDI intensity image at 23:59 UT on October 26, 2003 (represented by *contours*) is superposed on that at 23:59 UT on October 24 (*grey-scale image*). Both images are corrected for the solar differential rotation and projection effect. Letters 'S1' and 'S2' mark the two main leading negative sunspot groups, while 'N1' and 'N2' mark the two main following positive sunspot groups. The solid and dashed lines are drawn through the weighted centers of S1 and S2 and the two sunspots of N2 at 23:59 UT on October 24 and 26, respectively, to show the rotation of the sunspots. (b) MDI longitudinal magnetogram at 04:50 UT on October 26 (*grey-scale image*) superposed with the velocity map (*arrows*) derived from the MDI magnetograms at 04:50 UT and 05:50 UT on October 26, using the local correlation tracking (LCT) method.

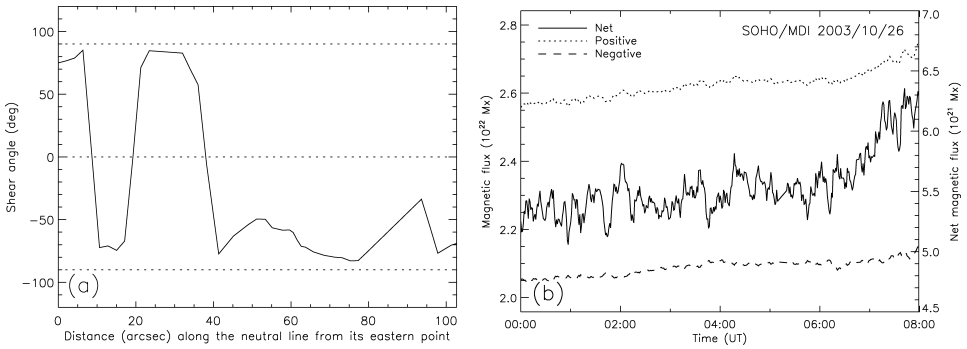

Figure 3. (a) Shear angle along the neutral line shown in Figure 1 (a) derived from HVVM observation at 02:33 UT. (b) Time profiles of the net (*solid*), positive (*dotted*), and negative (*dashed*) magnetic fluxes in AR 10486 in the period of 00:00–08:00 UT on October 26, 2003.

X-axis. The measured ψ from MDI intensity images at 23:59:33 UT of October 24 and 26 are 97° and 110°, respectively, i.e., these negative sunspots were rotated counter-clockwise by 13° (Figure 2(a)). Similar rotation was also observed for other sunspots, including the main positive sunspots N1 and N2, which were rotated counter-clockwise by about 30°. The magnetic features showed similar photospheric motions, as demonstrated, as an example, in Figure 2(b), in which we plot the MDI magnetogram at 04:50:03 UT overlaid with the velocity field that is derived by a local correlation tracking (LCT) method (November and Simon, 1988) using MDI magnetograms at 04:50:03 UT and 05:50:03 UT.

Sunspot motion and flux emergence increase the magnetic shear along the neutral line shown in Figure 1(a) as a solid thick line. The shear angles along the neutral line are plotted in Figure 3(a), from which we see that strong shear appeared in the north-west of N1 and N2. The maximum shear angle is 85.1° and the length of neutral line with shear angle larger than 80° is 14.3″ ($\approx 1.04 \times 10^4$ km), satisfying the sufficient conditions for a flare to take place proposed by Hagyard (1990).

Computed magnetic flux changes of AR 10486 with time are plotted in Figure 3(b). It shows that the positive flux increased with time more quickly than negative ones, leading to the increase of the net fluxes with time. The net flux in this AR was always positive, i.e., the positive flux was not balanced by the negative flux. These facts imply that the flux emergence was significant and some field lines in the region of positive polarity were connected to negative regions far out of AR 10486, as suggested by the 3D extrapolation shown in next section.

4. Magnetic Topology of the Active Region

We extrapolated the photospheric magnetic field obtained by THEMIS to infer the large scale 3D magnetic structure above the region. Before conducting the

extrapolation we inserted the THEMIS magnetogram at 08:55:52 UT (after correcting the differential rotation of the Sun) in a large MDI magnetogram at 07:15:03 UT to take advantage of the enhanced spatial resolution and spectropolarimetric accuracy of THEMIS. As described below, similar calibration properties of the magnetic field for the two instruments makes this possible. It was demonstrated that the correlation of the longitudinal magnetic field computed from the Na I 5896 Å line at 0.3Å (THEMIS) and the MDI magnetic field was rather good (nearly 1), especially in the spot umbra (Berlicki, Mein, and Schmieder, 2006). The magnetic field over the flare ribbons was not able to be computed, so that we used the interpolated values. The extrapolation of the magnetic field lines into the corona was performed with the assumption of a current-free field ($\vec{\nabla} \times \vec{B} = 0$), using the code developed by Démoulin *et al.* (1997). One might assume the validity of the topology derived with a potential field hypothesis in this complex active region. Theoretically, topology does not change if the extended non-linear force-free field (NLFFF) currents cover a volume right within a topological domain, e.g., all below the fan of a null point (Mandrini *et al.*, 1995). In the case of the existence of separatrices, Mandrini *et al.* (1995) found similar magnetic topology using a potential and a linear force-free field model. Antiochos, DeVore, and Klimchuk (1999) showed that the null point in his breakout model is still present with or without shear in the active region. Therefore, potential extrapolation presents us at least the essential large scale magnetic topology of the region to study the pre-events. We will discuss this point more in Section 6.

Figure 4 represents the extrapolation results, which clearly demonstrates that there exist two magnetic null points above the active region. One is rather high in the corona ($\approx$7.0 Mm) and another is just in the transition region ($\approx$ 2.25 Mm), as shown in Figure 4(a) and (b), respectively. The topology shows typical fan and spine structures. The fan structure of the high-altitude null point is partially depicted by the dark thin lines in Figure 4(c), while its spine field lines are connected to a far region and are not shown in Figure 4(c) except for the part close to the null point. The fan and spine structures of the low-altitude null point are depicted by the dark thick lines in Figure 4(c), and intersect with the photosphere in regions A, C, D, and G (see also Figures 5 and 6). It is also shown that the fan structure of the high-altitude null point intersect with the photosphere in regions A, B, F, and G.

5. TRACE Observational Results

5.1. TRACE IMAGES

This flare was well observed by TRACE. We present the TRACE 1600 Å image at 05:50:24 UT (before the X-ray flare onset) and the MDI magnetogram at 06:28 UT (just after the Hα flare maximum) in Figure 5. We marked eight regions with letters 'A' through 'H' in this figure, which we will study in detail below. This figure shows

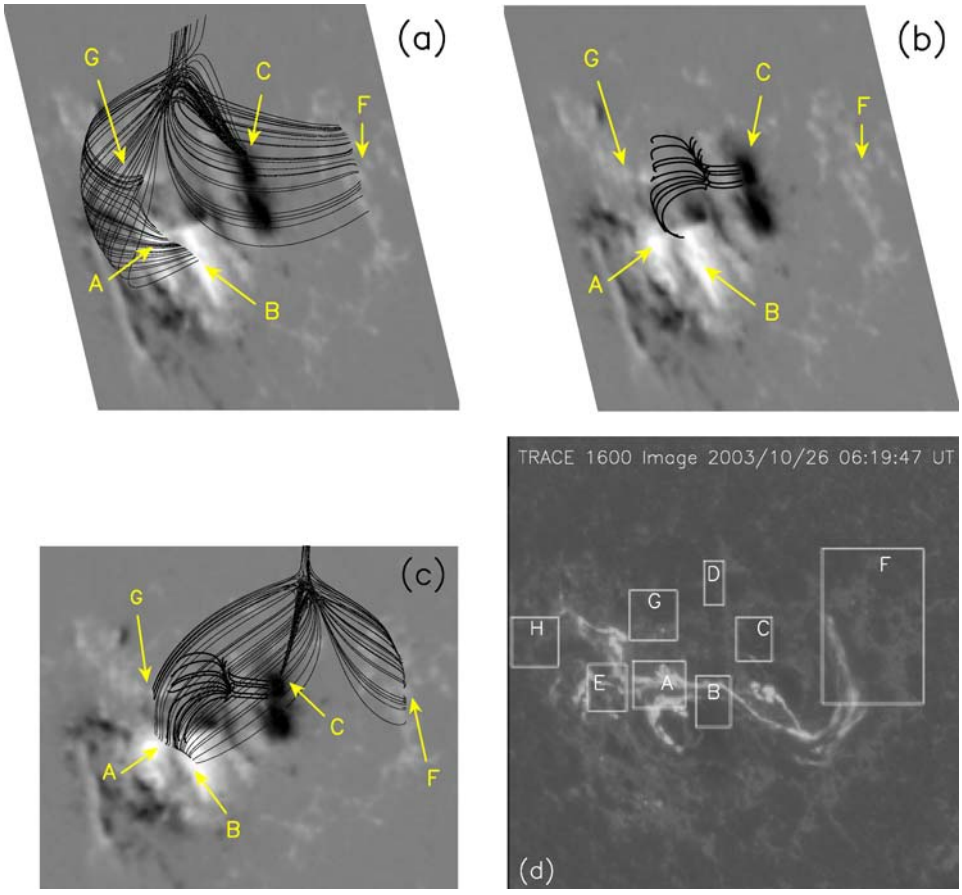

Figure 4. Extrapolated magnetic field lines using the longitudinal magnetic field observed by THEMIS at 08:55:52 UT for the active region NOAA 10486. The THEMIS magnetogram has been inserted in a large MDI map obtained at 07:15:03 UT ($390'' \times 390''$) to take advantage of high spatial resolution of THEMIS. The extrapolation was performed under the assumption of a current-free field. (a) A bird's-eye view of the high-altitude null, (b) A bird's-eye view of the low-altitude null, (c) A radial (*top*) view of both nulls, and (d) TRACE 1600 Å image at 06:19:47 UT. The *boxes* labeled 'A'–'H' indicate the eight regions we discuss in this paper.

that there were already TRACE 1600 Å bright patches in regions A, C, D, G, and E at 05:50:24 UT, while regions B and F did not display any brightening. However, TRACE 1600 Å movie reveals that regions B and F brightened quickly soon after the flare started. These observational facts are readily explained by the above 3D extrapolation, and suggest that the brightenings in TRACE 1600 Å before the flare onset are associated with the low-altitude null point rather than the high one (cf. Figure 4).

We show TRACE 1600 Å images at 05:49:49 UT and 05:57:14 UT, and 195 Å images at 05:49:43 UT and 05:58:51 UT in Figure 6, which are overlaid with MDI

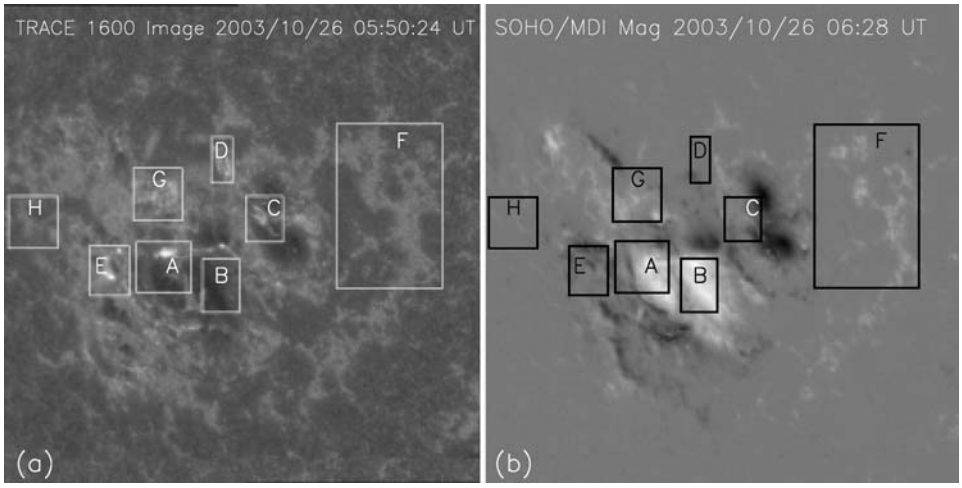

Figure 5. (a) TRACE 1600 Å image at 05:50:24 UT and (b) magnetogram at 06:28:03 UT observed by SOHO/MDI. *Letters* 'A'– 'H' have the same meaning as in Figure 4.

longitudinal magnetic field (contours) at 06:02:03 UT. Some regions are marked correspondingly to that in Figure 5. The TRACE 1600 Å image at 05:49:49 UT (Figure 6(a)) displays similar features as that at 05:50:24 UT (Figure 5(a)). Bright patches in C and D disappear in the image at 05:57:14 UT while those in regions A, E, and G only show slightly decreased emissions (Figure 6(b)). Regions C and D did not demonstrate strong emission later on and did not evolve in to main bright patches of the flare in 1600 Å, 195 Å (cf. Figure 7), and Hα (Li *et al.*, 2005). Meanwhile, a weak 1600 Å ribbon close to the main neutral line appeared in the image at 05:57:14 UT (Figure 6(b)), which evolved into the main bright ribbon of the flare in the impulsive and main phases. Above changes are not so obvious in TRACE 195 Å images at the corresponding times (Figure 6(c) and (d)). Brightness changes in regions A, C, and D are hardly discernible in 195 Å images at these two times, while brightness in regions E and G increased slightly (Figure 6(c) and (d), and cf. Figure 8).

5.2. TRACE LIGHT CURVES

We notice from Figures 5(a) and 6(a) that there were already some bright patches in TRACE 1600 Å images about 7 min before the X-ray flare onset (regions A, C, D, E, G and a region north to B), indicating that the chromosphere was heated to some extent in these regions. The locations of these regions with respective to the magnetic structures are shown in Figure 5(b). To study the flare evolution in these regions in both 1600 and 195 Å, we computed the average brightness of these regions in both 1600 and 195 Å at different times and plot the light-curves in Figure 7. It can be seen

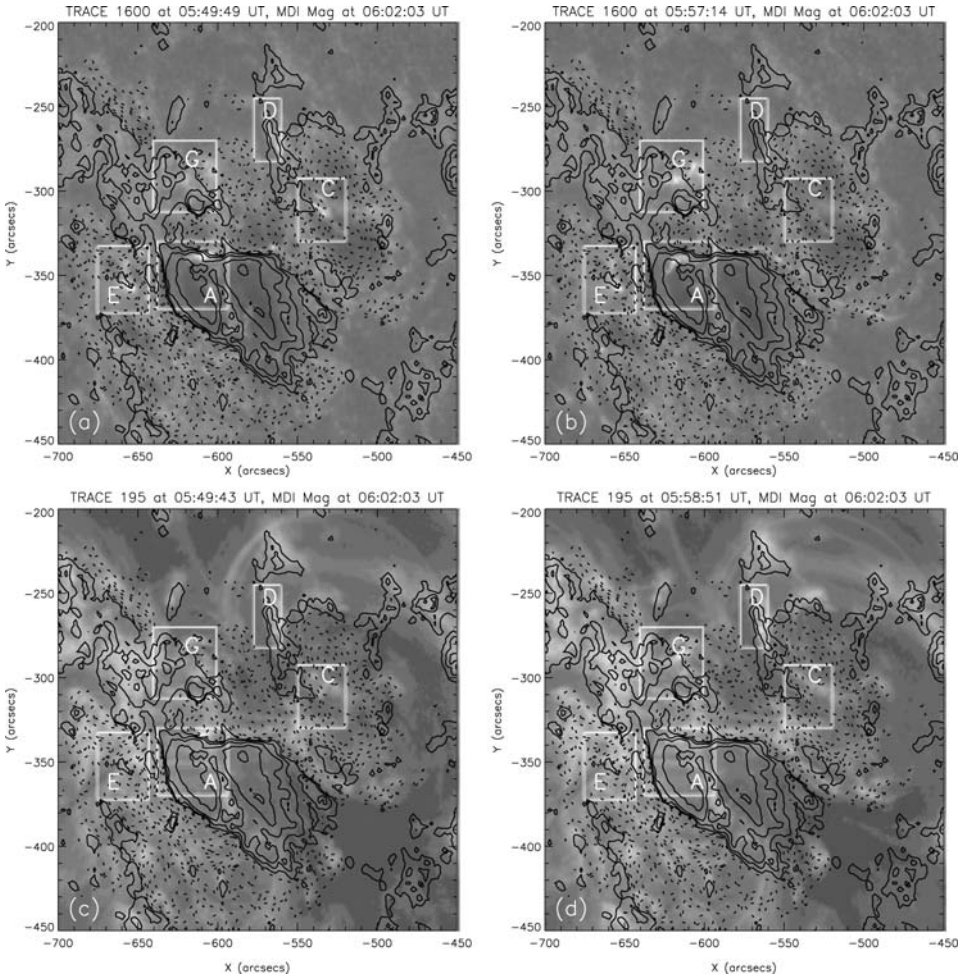

Figure 6. TRACE images in (a) 1600 Å at 05:49:49 UT, (b) 1600 Å at 05:57:14 UT, (c) 195 Å at 05:49:43 UT, and (d) 195 Å at 05:58:51 UT are overlaid with longitudinal magnetic field (*contours*) observed by SOHO/MDI at 06:02:03 UT. The *solid/dotted contours* stand for positive/negative magnetic polarities. *Letters* 'A'–'H' have the same meaning as in Figure 4.

that for each selected region, the light-curves in 1600 and 195 Å are similar in the impulsive phase and around the flare maximum before 07:20 UT. After 07:20 UT, emission in 1600 Å for the selected regions decreased to a very low level while that in 195 Å maintained at a relatively high level. For some of the selected regions, such as A and E, emission in 195 Å started to increase rapidly about 1–2 min later than in 1600 Å (see also Figure 8(a) and (d)). It is worth mentioning that region G behaves differently from other regions. It started to brighten almost at the same time as other regions but peaked much later, and retained emission in both 1600

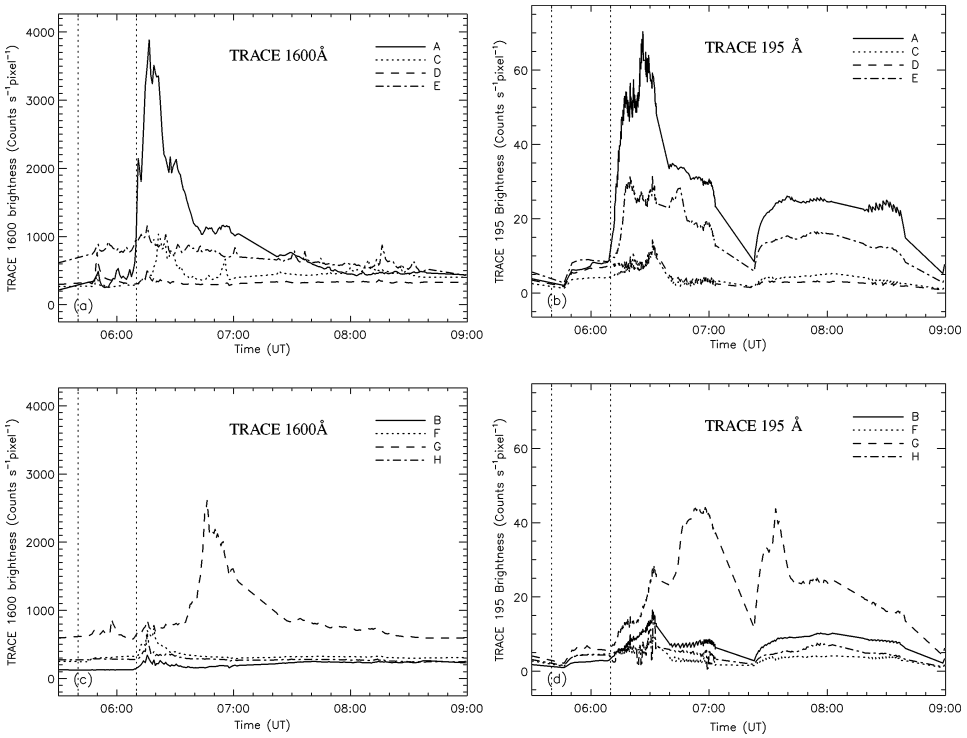

Figure 7. Time profiles of average brightness for the selected regions A, C, D, and E (see Figure 5) in (a) 1600 Å and (b) 195 Å from TRACE observation; (c) and (d) are the same as (a) and (b) but for regions B, F, G, and H. The two *dotted vertical lines* indicate the time range for the light-curves shown in Figure 8.

and 195 Å that was stronger than other regions except region A. Region G should correspond to the main GOES X-ray peak around 06:54 UT (Li *et al.*, 2005).

We plot light-curves for regions A, C, D, and E in both 1600 and 195 Å in a shorter time range (05:40–06:10 UT) in Figure 8 to study the EUV brightening before the main flaring process. It is clearly seen that all the four regions show enhanced emission around 05:50 UT in both 1600 and 195 Å (see also Figure 5(a)), implying that the atmosphere in these regions was heated to some extent, i.e., energy release occurred around 05:50 UT. Yet the released energy is just of small amount, which did not heat the flare atmosphere as violently as in the impulsive phase.

5.3. CURRENT

The vertical current density can be expressed as

$$J_z = \frac{1}{\mu_0}\left(\frac{\partial B_y}{\partial x} - \frac{\partial B_x}{\partial y}\right) \tag{1}$$

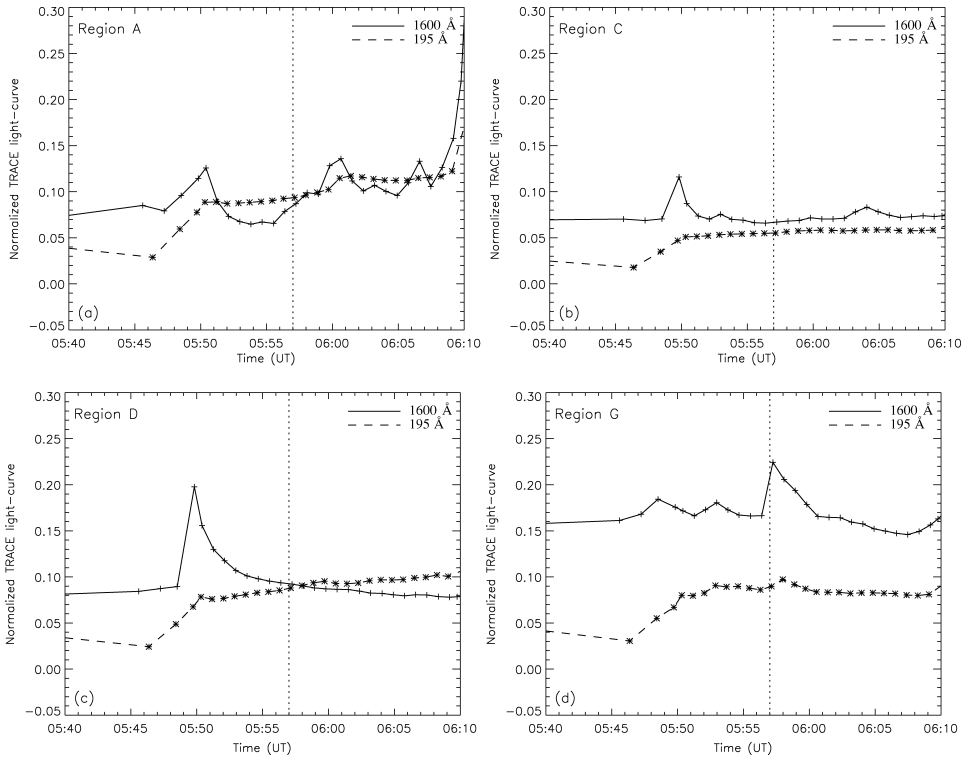

Figure 8. Time profiles of average brightness in the period of 05:40–06:10 UT (indicated by the two dotted vertical lines in Figure 7) in 1600 Å (*solid*) and 195 Å for (a) region A, (b) region C, (c) region D, and (d) region G shown in Figure 5 from TRACE observation. The *dotted vertical line* indicates the flare onset time in GOES X-rays.

where $\mu_0 = 4\pi \times 10^{-3}$ G m A^{-1} is the magnetic constant. We calculate J_z from observed vector magnetic field data. It is worth mentioning that J_z strongly depends on the solution of the 180 degree ambiguity for the transverse field. Incomplete elimination of the 180 degree ambiguity will introduce large uncertainty in J_z, and even yields erroneous values. It can be inferred from the above equation that strong current (large J_z) preferably appears in regions where the transverse field gradient is large, i.e., the transverse field changes quickly.

Figure 9(a) shows the TRACE 1600 Å image at 05:49:49 UT, which is overlaid with the longitudinal field (contours) from HVVM at 06:12 UT. The white bar indicates a cut in region C shown in Figures 5 and 6. Plotted in Figure 9(b) are the variations of TRACE 1600 Å intensity (Int) and the absolute transverse ($|B_t|$) and longitudinal ($|B_z|$) field strengths along the cut shown in frame (a). Figure 9(b) reveals that the peak value of TRACE 1600 Å emission appears close to the location where the transverse field changes significantly while the longitudinal field changes only slightly. In other words, bearing in mind that the active region

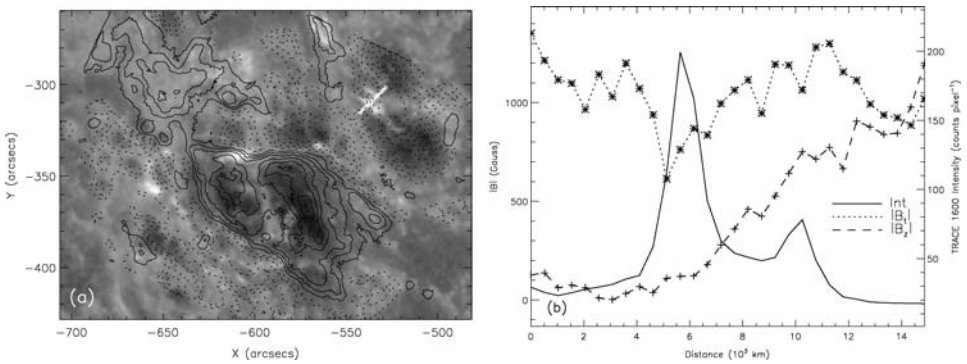

Figure 9. (a) Longitudinal magnetic field (*contours*) from HVVM at 06:12 UT is overlaid on TRACE 1600 Å image at 05:49:49 UT. The contour levels are ±80, 200, 400, 800, 1200, 1600, 2000 Gauss. (b) Variations of TRACE 1600 Å intensity (I_{1600}, *solid*), and the transverse (*dotted*) and longitudinal (*dashed*) magnetic field strength along the cut shown in frame (a) as a white bar corresponding to region C.

location is S15E44 and taking into account the projecting effect, the heated plasma producing 1600 Å emission spatially corresponds to large current density, and to the intersections of separatrix related to the low-altitude null point with the planes of the chromosphere and the photosphere (see Section 4). We also noticed that this region is located far away from the main eruption site and has certainly no relationship with the X1.2 flare (Figure 4(d)).

6. Discussion and Conclusion

We studied the precursors of the 3B/X1.2 flare of October 26, 2003, occurring in the AR 10486. We take advantage of high temporal and spatial resolutions of TRACE observation and high polarimetry sensitivity of THEMIS to relate the magnetic topology of the active region and the EUV brightenings observed before the flare. The TRACE 1600 Å bright patches are good tracers, in the photosphere, of the locations where the energy release can produce plasma heating.

Magnetic field evolution shows that the AR 10486 is characterized by continuous flux emergence, sunspot motion and rotation, leading to the formation of its δ configuration. The magnetic shear increases along the neutral line (Figure 1(a)) to a value fulfilling the sufficient conditions for getting flares (Hagyard, 1990).

The temporal variations of magnetic flux in the region reveal that the positive flux exceeded the negative flux, yielding positive net flux in the region. This could be explained by the fact that some of the field lines in this region, such as the spine field lines of the high-altitude null point, are connected to far regions north-west to AR 10486, as demonstrated by the 3D extrapolation of the longitudinal magnetic field from THEMIS observation (Figure 4). On the other hand, even though we

corrected the magnetic field data for the differential rotation of the Sun, it may still introduce some uncertainty in the computed magnetic fluxes.

The 3D extrapolation was performed with the assumption of current-free field to study the large scale topology of AR 10486. The extrapolation results suggest the existence of two magnetic nulls above this active region, and clearly show the corresponding fan surfaces and spine structures (Figure 4), which are typical topology near a null point (Filippov, 1999; Antiochos, 1998; Aulanier *et al.*, 2000). It has been demonstrated that this method of extrapolation is theoretically and observationally valid. Indeed magnetic topology is not changed if the extended non-linear force free field currents cover a volume that is located right within a topological domain, e.g., all below the fan of a null point. This approximation was also used with success for the study of pre-eruptive-flare topologies (Schmieder *et al.*, 1997; Aulanier *et al.*, 2000; Maia *et al.*, 2003; Manoharan and Kundu, 2003; Gary and Moore, 2004) which is somehow justified because it is known that at large enough altitudes, the field tends to be potential (Schmieder *et al.*, 1996). Large scale reconnection like the breakout model in a quadrupolar configuration (Antiochos, 1998) should be detectable if it was present. A detail investigation of this possibility of reconnection was performed by looking at the precursor brightenings in TRACE 1600 Å before the X 1.2 flare, used as tracers of the heating produced by the reconnection.

TRACE 1600 Å images display several bright areas before the flare onset (Figures 5 and 6, regions A, C, D, E and G). The brightness of these regions shows quick increase around 05:50 UT in both 1600 and 195 Å (Figures 7 and 8). Even though the brightness at this time is much weaker than in the main phase of the flare, the quick increase presumably implies that the atmosphere in these regions at this time was heated to some extent, i.e., there should be energy deposition in these regions. The 3D magnetic extrapolation reveals that these regions are located around the intersections of the fan surface and the spine structure of the low-altitude null point with the planes of the photosphere and the chromosphere. Coupling with the topology from the 3D extrapolation (Figure 4), the time profiles of brightness of these regions (Figures 7 and 8), and the distributions of TRACE 1600 Å intensity and magnetic field strengths along the selected cut (Figure 9), the enhanced brightness (emission) in these regions provides evidence for the magnetic reconnection near the low-altitude null point. This is supported by the fact that bright patches were not observed in regions B and F before the flare onset. However, this reconnection and brightness enhancement have no direct relation with the main flare.

On the other hand, no bright patch was observed corresponding to the high-altitude null point before the flare. But just after the flare, bright TRACE 1600 Å patches corresponding to the high-altitude null point, including brightening in regions B and F, were observed, suggesting that magnetic reconnection occurred near the high-altitude null point at the flare time due to the eruption of lower magnetic field lines, which leads to the opening of the coronal magnetic field lines. Therefore,

the opening of the coronal lines is just a byproduct of the large 3B/X1.2 flare rather than its trigger. This warns us that one should be very cautious to interpret observed flare precursors.

We show that the existence of the two null points has no crucial role in triggering the main flare. The magnetic structure might lose its equilibrium under the influence of strong and increasing shear as proposed in some flare models (Isenberg, Forbes, and Démoulin, 1993; Lin, Forbes, and Isenberg, 2001). In these models, the rising structure reconnects with the overlying magnetic field, leading to the enhancement of the intensity of large structures. The bright patch of region F in our case can be taken as the signature of such a reconnection event. The pre-flare events of the X1.2 flare on October 26 were not precursors of this large flare. On the following days low null points in the corona were also observed in the active region, leading to small flares. It has been shown that large flares were produced independent of the presence of the null points (Mandrini *et al.*, 2006). One pre-flare event of the X17.2 flare of October 28, 2003, that occurred in the same active region was recognized to be a precursor of the main flare, opening the overlying field lines by an eruption of underlying field lines before the main energy release.

Therefore, we conclude that eruptions can be triggered without pre-eruptive coronal null point reconnection, and the presence of magnetic null points does not necessarily lead to the occurrence of flares. Large flares can occur without a pre-flare reconnection of the coronal magnetic field lines like in the breakout model even if null points do exist.

Acknowledgements

We thank P. Mein for his help and discussion on THEMIS/MSDP data processing and analysis. We are also grateful to the THEMIS team which operates the telescope at Tenerife and to the Huairou colleagues for providing the vector magnetic field data. SOHO is a joint project of ESA and NASA, and THEMIS is a French-Italian telescope operated on the island of Tenerife by the CNRS-CNR in the Spanish Observatorio del Teide of the Instituto de Astrofísica de Canarias. The magnetic field extrapolations used in this paper were performed with the code based on FRench Online MAGnetic Extrapolations (FROMAGE). FROMAGE is a joint project between LESIA (Observatoire de Paris), CPhT (Ecole Polytechnique), and the Centre National d'Etudes Spatiales (CNES). The work of HL was supported by the National Natural Science Foundation of China (NSFC, grant number 10273023, 10333040 and 10573038) and National Basic Research Priorities Project (G2000078402) of China, and that of AB and BS by the European Commission through the RTN programme (European Solar Magnetism Network, contract HPRN-CT-2002-00313). This work was partially supported by the French–Chinese contract (CNRS-CAS No. 16304).

References

Ai, G.X. and Hu, Y.F.: 1986, *Publ. Beijing Astron. Obs.* **8**, 1.
Ambastha, A., Hagyard, M.J., and West, E.A.: 1993, *Solar Phys.* **148**, 277.
Antiochos, S.K.: 1998, *Astrophys. J.* **502**, L181.
Antiochos, S.K., DeVore, C.R., and Klimchuk, J.A.: 1999, *Astrophys. J.* **510**, 485.
Aulanier, G., DeLuca, E.E., Antiochos, S.K., McMullen, R.A., and Golub, L.: 2000, *Astrophys. J.* **540**, 1126.
Aulanier, G., Pariat, E., and Démoulin, P.: 2005, *Astron. Astrophys.* **444**, 961.
Berlicki, A., Mein, P., and Schmieder, B.: 2006, *Astron. Astrophys.* **445**, 1127.
Craig, I.J.D. and Fabling, R. B.: 1996, *Astrophys. J.* **462**, 969.
Craig, I.J.D., Fabling, R.B., Heerikhuisen, J., and Watson, P.G.: 1999, *Astrophys. J.* **523**, 838.
DeVore, C.R. and Antiochos, S.K.: 2005, *Astrophys. J.* **628**, 1031.
Domingo, V., Fleck, B., and Poland, A.I.: 1995, *Solar Phys.* **162**, 1.
Démoulin, P., Bagala, L.G., Mandrini, C.H., Hénoux, J.C., and Rovira, M.G.: 1997, *Astron. Astrophys.* **325**, 305.
Démoulin, P. and Klein, K.-L.: 2000, in J.-P. Rozelot, L. Klein, and J.-C. Vial (eds.), *Transport and Energy Conversion in the Heliosphere, Lecture Notes in Physics*, Vol. 553, Springer-Verlag, Berlin, p. 99.
Filippov, B.: 1999, *Solar Phys.* **185**, 297.
Gary, G.A and Moore, R.L.: 2004, *Astrophys. J.* **611**, 545.
Hagyard, M.J.: 1990, *Mem. Soc. Astron. Ital.* **61**, 337.
Handy, B.N. *et al.*: 1999, *Solar Phys.* **187**, 229.
Isenberg, P.A., Forbes, T.G., and Démoulin, P.: 1993, *Astrophys. J.* **417**, 368.
Ji, H.S. and Song, M.T.: 2001, *Astrophys. J.* **556**, 1017.
Li, H., Sakurai, T., Ichimoto, K., and UeNo, S.: 2000, *Publ. Astron. Soc. Japan* **52**, 465.
Li, H. *et al.*: 2005, *Chinese J. Astron. Astrophys.* **5**, 645.
Lin, J., Forbes, T.G., and Isenberg, P.A.: 2001, *J. Geophys. Res.* **106**, 25053.
Maia, D., Aulanier, G., Wang, S.J., Pick, M., Malherbe, J.-M., and Delaboudinière, J.-P.: 2003, *Astron. Astrophys.* **405**, 313.
Mandrini, C., Démoulin, P., Rovira, M.G., de La Beaujardiere, J.-F., and Hénoux, J.C.: 1995, *Astron. Astrophys.* **303**, 927.
Mandrini, C.H. *et al.*: 2006, *Solar Phys.* in press.
Manoharan, P.K. and Kundu, M.R.: 2003, *Astrophys. J.* **592**, 597.
Manoharan, P.K. and Kundu, M.R.: 2005, *Adv. Space Res.* **35**, 70.
Mein, P.: 2002, *Astron. Astrophys.* **381**, 271.
Ning, Z.J. *et al.*: 2006, *Astrophys. Space Sci.* (submitted).
November, L.J., and Simon, G.W.: 1988, *Astrophys. J.* **333**, 427.
Qiu, K.P., Yeh C.T., Zhou, G.P., Li, H., and Fang C.: 2006, *Chinese J. Astron. Astrophys.* (submitted).
Sakurai, T. *et al.*: 1992, *Publ. Astron. Soc. Japan* **44**, L123.
Scherrer, P.H. *et al.*: 1995, *Solar Phys.* **162**, 129.
Schmieder, B., Démoulin, P., Aulanier, G., and Golub, L.: 1996, *Astron. Astrophys.* **467**, 881.
Schmieder, B. *et al.*: 1997, *Astron. Astrophys.* **325**, 1213.
Schmieder, B. and van Driel, L.: 2005, in K.P. Dere, J. Wang, and Y. Yan (eds.), *Coronal and Stellar Mass Ejections, IAU Symp.* **226**, 149.
Wang, H.M., Ewell, Jr, M.W., Zirin, H., and Ai, G. X.: 1994, *Astrophys. J.* **424**, 436.
Zhang, H.Q. *et al.*: 2003, *Chinese J. Astron. Astrophys.* **3**, 491.